Catalysis Today 141 (2009) 355–360

Contents lists available at ScienceDirect

Catalysis Today

journal homepage: www.elsevier.com/locate/cattod

Effect of the titania morphology on the Au/TiO_2-catalyzed aerobic epoxidation of stilbene

Pascal Lignier [a], Massimiliano Comotti [b], Ferdi Schüth [b], Jean-Luc Rousset [a], Valérie Caps [a,*]

[a] Institut de recherches sur la catalyse et l'environnement de Lyon (IRCELYON, CNRS-Université de Lyon), 2 avenue Albert Einstein, F-69626 Villeurbanne Cedex, France
[b] Max-Planck-Institut für Kohlenforschung, Kaiser-Wilhelm-Platz 1, D-45470 Mülheim a.d. Ruhr, Germany

ARTICLE INFO

Article history:
Available online 13 June 2008

Keywords:
Gold
Nanoparticles
Titania
Epoxidation
Aerobic

ABSTRACT

We use a colloidal deposition method to prepare gold nanoparticles with similar size distributions centered at 3 nm over various anatase titania supports. All UV100, PC500 and AK350 titanias are loaded with similar amount of gold (1.0 ± 0.2 wt.%) which is in similar electronic and optical environments, as shown by X-ray photoelectron spectroscopy (XPS) and UV–vis. This allows us to assess the effect of the titania crystallization, morphology and chemical composition on the catalytic properties of gold in the aerobic epoxidation of *trans*-stilbene. We find that Au/UV100 is more active than Au/PC500 and Au/AK350 but that selectivities are similar on all materials. Epoxide yields on the other hand critically depend on the support functionalization and surface composition. TG–DTA characterization of the bare titania powders reveals indeed that AK350, which leads to the least active catalyst, is slightly less hydroxylated than PC500 and UV100. This indicates that surface titanol groups might be involved in the epoxidation of *trans*-stilbene. The presence of boron oxide on Au/UV100 (XPS), due to reaction of UV100 with the $NaBH_4$ reductant during the synthesis, is also thought to promote the epoxide-forming mechanism. This chemical promotion effect appears to compensate for the specific and beneficial gold–P25 interaction. As a result, Au/UV100 is more efficient than the reference Au/P25 catalyst for this reaction.

1. Introduction

Epoxidations of substituted alkenes are key-reactions of the fine chemical industry; the oxygenated products they provide are essential intermediates for the chemical syntheses of more sophisticated molecules. Although epoxidations of lower alkenes have been carried out since the 1980s over the well-known microporous titanium silicalite TS-1 (Enichem) [1,2], the heterogeneous epoxidations of larger alkenes have relied on the synthesis of titanium-based structures with larger pores [3–5]. However, if stability of the porous catalyst is not the main issue, reactions involving the bulkiest olefins still suffer from diffusional limitations due to confinement of the active site within deep inorganic cavities. In addition, these materials usually require the use of organic oxidants (e.g. *tert*-butyl hydroperoxide), which are less environmentally friendly than the hydrogen peroxide associated with TS-1. This has its importance, considering that these hazardous oxidizing agents are used in stoichiometric amounts or even in excess, since epoxide yields on peroxides are quantitative [1]. One structure should be mentioned though, where the environment of the catalytic site is made more hydrophobic, just like in TS-1, in order to allow the use of H_2O_2 as oxidant [6,7]. However, the synthesis of these complex structures from expensive titanium precursors is not straightforward and probably difficult to scale-up.

When looking into cleaner, safer and simpler alternatives to these epoxidation processes of larger alkenes, we found that supported gold nanoparticles could epoxidize *trans*-stilbene in methylcyclohexane using air as principal oxidant [8]. In particular, the Au/TiO_2 reference catalyst [9] from the World Gold Council (WGC) exhibited higher activity and selectivity than the reference Au/C-WGC [10]. However, the P25 support used is a low surface area titania that does not disperse well within the apolar reaction medium. Although it is accepted that P25 is the optimum support for gold in the oxidation of CO, we found that it might not be appropriate for oxidations in the liquid phase and that testing higher surface area titanias could be interesting.

In this paper, we make use of a colloidal deposition method developed by Comotti et al. [11] to prepare similar gold particle size distributions over various titania supports, including high surface area materials. The key-idea of this technique is the synthesis of a gold sol with a narrow size distribution *before*

* Corresponding author. Tel.: +33 472 445 331; fax: +33 472 445 399.
E-mail address: valerie.caps@ircelyon.univ-lyon1.fr (V. Caps).

0920-5861/$ – see front matter © 2008 Elsevier B.V. All rights reserved.
doi:10.1016/j.cattod.2008.04.032

deposition on the support. This method thus allows to assess the effect of the support in catalytic reactions by isolating it from other parameters such as metal dispersion and particle size effect. This methodology has already been used successfully to demonstrate support effects in the gas phase CO oxidation reaction [11]. In the present study, we will show how the gold-catalyzed epoxidation of stilbene in the liquid phase is influenced by the titania morphology/surface composition. In order to rationalize these observations, the effect of the nature of the titania on the catalyst preparation, and especially on the electronic, optical and morphological properties of the supported gold nanoparticles, will be discussed.

2. Experimental

2.1. Preparation of the catalysts

The catalysts were prepared according to the method described in Ref. [11], using commercially available 100% anatase titanias and poly(vinylalcohol) as the protecting agent. A gold loading of 1 wt.% is intended on all supports. The supports have the following characteristics:

- TiO_2-AK350: Tronox A-K-350, $>250\ m^2\ g^{-1}$.
- TiO_2-PC500: Millenium Chemicals PC500, $>250\ m^2\ g^{-1}$.
- TiO_2-UV100: Sachtleben Chemie GmbH Hombikat UV100, $>250\ m^2\ g^{-1}$.

Basically, a solution of the protecting agent (Au/PVA = 1.5:1 mg mg^{-1}) is added to an aqueous solution of gold (100 mg L^{-1}) at room temperature under vigorous stirring (1250 rpm). The mixture is stirred for 10 min. An aqueous solution of sodium borohydride 0.1N (Au/$NaBH_4$ = 1:5 mol mol^{-1}) is then added, which makes the solution turn dark brown-red, indicating the formation of a gold sol. The support (1 g) is introduced upon stirring. Stirring is carried on until total adsorption of the gold sol onto the support, as indicated by discoloration of the solution (followed by UV–vis). After filtration, extensive washing (H_2O/1 L), the resulting powder is dried in air at 90 °C. All these steps are carried out in the absence of light by covering all containers with aluminum foil. All catalysts are calcined in air at 250 °C for 4 h prior to characterization and catalytic testing.

2.2. Characterization

Chemical analyses of the samples are carried out in-house by inductively coupled plasma optical emission spectroscopy (ICP-OES Activa from HORIBAJobin Yvon) to determine the gold loadings. The S contents of the titania supports are measured at the Service Central d'Analyse (Solaize, France), by infrared titration of SO_2 after combustion of the sample at 1800 °C in flowing oxygen.

BET surface areas and pore volumes are determined on N_2 adsorption/desorption isotherms collected at liquid nitrogen temperature using a Micromeretics ASAP 2010 apparatus. Before the measurement, ~50 mg of the titania powder is dehydrated under vacuum at 300 °C overnight.

X-ray diffraction (*XRD*) of the supports are carried out on a Bruker (Siemens) D5005 diffractometer. The XRD patterns are collected using Cu $K_{\alpha 1+\alpha 2}$ radiations (λ = 1.54184 Å) over a 2θ range of 3–80° at a rate of 0.02° s^{-1}. The average size of the titania crystallites is calculated according to the Scherrer equation.

Thermogravimetric/differential thermal analyses (*TG–DTA*) are carried out on a Setaram Instrumentation SETSYS Evolution-1200 apparatus. Samples are heated in flowing air (50 $cm^3\ min^{-1}$) from 20 to 600 °C at 10° min^{-1}.

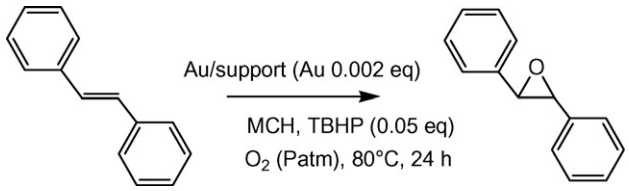

Scheme 1. Reaction conditions for the epoxidation of *trans*-stilbene over gold catalysts.

Transmission electron microscopy (*TEM*) is performed on a JEOL 2010 F microscope operating at 200 kV, equipped with a field emission gun and a high-angle annular dark field detector. Size distributions are obtained on bright field images.

X-ray photoelectron spectroscopy (*XPS*) experiments are carried out on a Kratos Axis Ultra DLD spectrometer using monochromated Al Kα X-rays (1486.6 eV, 150 W), a pass energy of 10 eV, a hybrid lens mode and an indium sample holder in ultra-high vacuum ($P < 10^{-9}$ mbar). The analyzed surface area is 700 μm × 300 μm. Charge neutralization is required for all samples. The peaks (O 1s, Au 4f, Ti 2p, S 2p, B 1s, Na 1s) are referenced to the C–(C, H) components of the C 1s band at 284.6 eV. Shirley background subtraction and peak decomposition using Gaussian–Lorentzian products are performed with the Vision 2.2.6 Kratos processing program. A degree of asymmetry is added to fit the Au 4f peaks.

UV–vis diffuse reflectance spectroscopy: UV–vis analyses of the powder samples are performed on a PerkinElmer Lambda 35 UV–vis spectrometer equipped with a Labsphere RSA-PE-20 diffuse reflectance accessory. UV spectra are recorded in the range 190–1100 nm with a scan speed of 240 nm min^{-1} and a slit width of 2 nm. The incident beam is 8° off axis from the sample holder in order to eliminate specular reflection.

2.3. Catalytic evaluation

The catalytic tests are carried out in magnetically stirred (900 rpm) glass batch reactors held at 80 °C for 24 h in air at atmospheric pressure. The reaction mixtures consist of substrate (*trans*-stilbene, 96%, 186 mg/1 mmol), solvent (methylcyclohexane, MCH, 99%, 20 mL/155 mmol), catalyst (2.1 ± 0.1 μmol Au) and *tert*-butylhydroperoxide (70% TBHP in H_2O, 7 μl/0.05 mmol). *Trans*-stilbene conversion (*C*, %), epoxide yield (*Y*, %) and selectivity (*S*, %), which have been explicitly defined elsewhere [10], are determined by HPLC-product analysis. Selectivity is defined as the (epoxide yield)/(tS conversion) ratio (×100). It is noted that *trans*-stilbene oxide (the epoxide) is the main product of the reaction. Only traces of benzil and benzaldehyde are detected. The remaining *trans*-stilbene conversion is accounted for by the formation of HPLC-undetectable total oxidation products, such as carbon dioxide [10] (Scheme 1).

3. Results

3.1. Characteristics of the supports

All supports have been characterized by XRD, BET and ICP in order to determine the size of the titania crystallites, the specific surface area and pore volume and the sulfur content. Results are given in Table 1. All supports are essentially made of anatase crystallites. These pure anatase supports all contain some sulfur, which comes from the titanium precursor used. PC500 and UV100 exhibit the highest sulfur contents.

It is interesting that, whatever the average crystallite size calculated from the Scherrer equation on diffractograms of the supports (5–9 nm), the specific surface areas and pore volumes

Table 1
Physico-chemical properties of the titania supports

Support	Crystallographic phase (average crystallite size in nm)	Specific surface area ($m^2\ g^{-1}$)	Pore volume ($cm^3\ g^{-1}$)	S content (wt.%)
TiO_2-AK350	100% anatase (5)	330	0.33	0.40
TiO_2-PC500	100% anatase (7)	340	0.35	0.64
TiO_2-UV100	100% anatase (9)	340	0.34–0.38 [14,15]	0.68

measured are similar. This indicates a marked difference in the titanias morphology/structuration. Given that isolated anatase spheres of 3.9 g cm^{-3} theoretical density and 5 nm diameter would display a surface area of 310 $m^2\ g^{-1}$, it can be concluded that AK350 is pretty well-crystallized under this form. On the other hand, anatase spheres of 7 and 9 nm diameter would yield theoretical surface areas of 220 and 170 $m^2\ g^{-1}$, respectively. The 340 $m^2\ g^{-1}$ specific surface areas measured for PC500 and UV100 could be an indication that the broadening of the XRD peaks in these samples arises more from the presence of bigger, poorly crystallized and amorphous titania particles and thus that these supports might possess an intra-particle porosity. These supports are indeed mesoporous with mean pore diameters of ~5.6 nm for UV100 [12] and 6.1 nm for PC500 [13].

All the supports have also been characterized using TG–DTA. The TG patterns of the titanias (Fig. 1) basically exhibit one endothermic peak with a maximum in the range 90–100 °C associated with weight losses reported in Table 2. This is attributed to dehydration of the oxide powder as already discussed elsewhere [16]. Additional weight loss in the range 150–600 °C (Table 2) essentially comes from dehydroxylation of the support [16]. Total weight losses vary between 13–15%. Given that all the supports exhibit similar surface areas, it can be concluded that AK350 is somewhat less functionalized than PC500 and UV100, i.e. that the density of surface water and titanol groups on AK350 is lower than on the two other anatase supports. However, if one considers the weight loss after 250 °C (all the catalysts have been calcined at this temperature) it should be noted that all supports exhibit a similar functionalization state (2.1-2.3%), as the majority of the titanol and hydroxyl groups have been lost before 250 °C

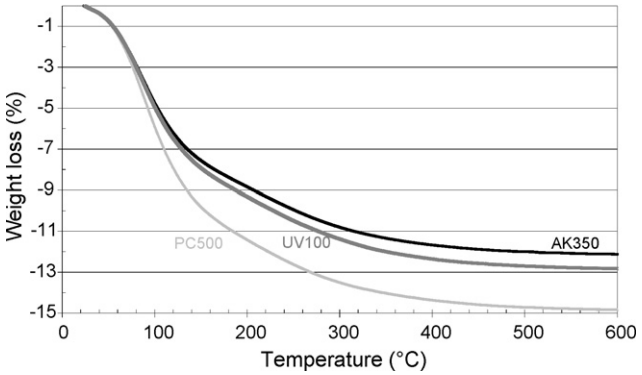

Fig. 1. TG–DTA patterns of the bare titania supports.

Table 2
Weight losses and catalytic behaviors of the titania supports

Support	Weight loss (%)			Catalytic properties		
	20–150 °C	150–600 °C	250–600 °C	*C* (%)	*Y* (%)	*S* (%)
TiO_2-AK350	7.9	4.6	2.1	<1	<1	<1
TiO_2-PC500	10.2	4.7	2.3	<1	<1	<1
TiO_2-UV100	8.5	4.3	2.3	15	2	13

In summary, AK350 is a high surface area titania made of small, well-crystallized anatase particles. On the other hand, PC500 and UV100 exhibit high surface area, high surface functionalization and similar concentrations of sulfur.

3.2. Catalysts

The physico-chemical properties of the Au/TiO_2 materials are shown in Tables 3 and 4. All concern the calcined samples, except the Au/Cl surface atomic ratios derived from an XPS study of the uncalcined materials.

3.2.1. Chemical composition (chemical analysis)

It can be seen that the desired 1.0 ± 0.2 wt.% gold loadings are achieved on all supports and that it is slightly higher on PC500 and UV100 (Table 3). This is attributed to the intense hydration/hydroxylation of the bare PC500 and UV100 supports (which is lost upon drying and calcination steps of the preparation). Sodium has also been found in high concentration in Au/AK350 (0.2 wt.%), which gives an Au/Na molar ratio of 0.54. On the other hand, less than 200 ppm Na are measured in Au/PC500 and Au/UV100.

3.2.2. Morphology (TEM)

The average gold particle size (3.0 ± 0.2 nm) is similar on all titanias. Also particle size distributions are rather similar (Fig. 2) with ~75% of the counted particle having diameters between 1 and 3 nm. It is noted that the particle size distributions presented here take into account more than 96% of the counted particles. Less than 4% of the particles found indeed exhibit a diameter above 10 nm. The average particle sizes of gold (and standard deviations) are however calculated by taking into account the whole distribution (100% of the particles).

The resulting dispersions of gold (Table 3) are calculated from the average particle size by assuming a cubo-octahedron shape of the particle [17].

3.2.3. Optical properties (UV–vis DRS)

The 400–800 nm region of the UV–vis Kubelka–Munk [18] transformed diffuse reflectance spectra of the samples is presented

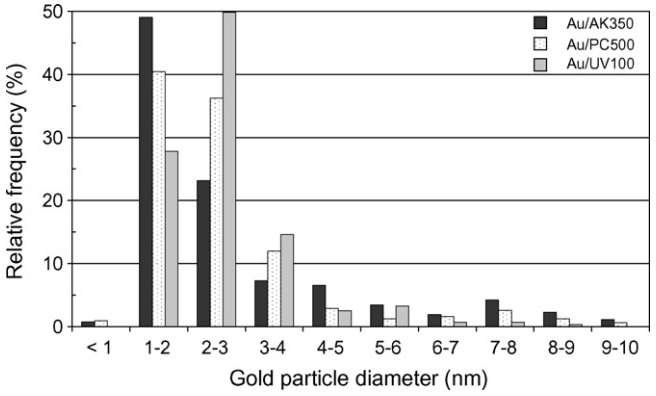

Fig. 2. Particle size distributions of gold dispersed on AK350, PC500 and UV100 titanias via the colloidal deposition method.

Table 3
Physico-chemical and catalytic properties of the Au/TiO_2 materials

Catalyst	Au loading (wt.%)	Average Au particle size (nm)[a]	Gold dispersion (%)	Gold plasmon band (nm)	Catalytic properties			
					C (%)	*Y* (%)	*S* (%)	TON[b]
Au/TiO_2-AK350	0.93	3.1 (2.5)	41	542	26	20	75	300
Au/TiO_2-PC500	1.10	2.9 (2.4)	43	550	38	29	75	430
Au/TiO_2-UV100	1.21	2.8 (2.4)	45	550	64	44	69	680
Au/TiO_2-WGC	1.5	3.7 (1.5)	36	570	42	27	64	620

[a] The average particle size of gold are calculated by taking into account the whole distribution derived from TEM studies. In brackets are the standard deviations.
[b] TON stands for turnover number, i.e. the number of mole of *trans*-stilbene converted per mole of surface gold in 24 h.

Table 4
XPS data of the Au/TiO_2 materials

Catalyst	Binding energies (eV)				Surface atomic ratios				
	Au $4f_{7/2}$	Ti $2p_{3/2}$	Cl $2p_{3/2}$[a]	S $2p_{3/2}$	Au/Ti	Au/Cl[a]	Au/S	Au/Na	Au/B
Au/TiO_2-AK350	82.8 ($Au^{\delta-}$)	458.4	198.0	168.4[a]	0.039	4.0	3[a]	0.24	–
Au/TiO_2-PC500	83.1 ($Au^{\delta-}$)	458.5	198.2	168.3	0.025	5.6	12	–	–
Au/TiO_2-UV100	83.0 ($Au^{\delta-}$)	458.4	198.2	168.2	0.024	4.0	6	–	2.3
Au/TiO_2-WGC	83.0 ($Au^{\delta-}$)	458.4	–	–	0.015	–	–	Min. 3[b]	–

[a] Obtained on the uncalcined materials.
[b] Estimation based on the bulk molar ratio.

in Fig. 3. It exhibits the typical surface plasmon of gold nanoparticles. The surface plasmon resonances of Au/UV100 and Au/PC500 are very similar, at 550 nm (Table 3), showing the similar size, shape and environment of the gold particles in these two catalysts. The shift to 542 nm of the band maximum in Au/AK350 is related to the different morphology of the AK350 support and the different chemical environment of gold, due to the presence of sodium on the catalyst surface, as will be shown in the following section. The red-shift in the plasmon resonance of the reference Au/TiO_2-WGC catalyst (~570 nm) is attributed to the higher refractive index of the highly crystallized P25 support [19], which is made of 25 nm anatase crystallites (80%) and 40 nm rutile crystallites (20%). The overall different shape of the plasmon resonance illustrates the specific environment of gold particles on P25 titania in the reference catalyst.

3.2.4. Electronic properties (XPS)

The Au $4f_{7/2}$ core level (Table 4) is slightly shifted, in all samples, towards a lower binding energy than that of bulk Au^0, which is reported to be at 84.0 eV [20–22]. This is attributed to a charge transfer from the titania supports to the gold particles, as it exceeds

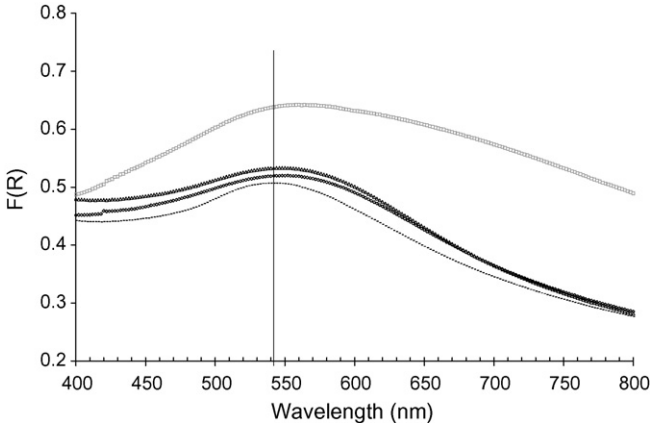

Fig. 3. UV–vis Kubelka–Munk transformed diffuse reflectance spectra of the catalysts (gold plasmon band region): Au/AK350, Au/UV100, Au/PC500, Au/TiO_2-WGC (from bottom to top on the *y* axis).

the extent of the surface core level shift (−0.4 eV) that could be expected from the nanometric size of the gold particles [23,24]. The binding energy of gold is similar on all supports (83.0 ± 0.2 eV), indicating similar metal–support interactions in all materials.

The binding energy of Ti $2p_{3/2}$ (Table 4) is shifted towards a lower value than that normally reported for bulk TiO_2 (458.6 eV [25] to 458.8 eV [26] and even 459.0 eV [27]). The extent of the shift (max. −0.2 eV) is however not significant and lower values of the Ti $2p_{3/2}$ binding energy have been reported in some cases (457.6 eV [28]), particularly for sulfur-doped titania (458.2 eV [29]).

It is interesting that, for similar gold dispersions (42–45%), the Au/Ti surface atomic ratio is higher on AK350 (0.039) than on UV100 and PC500 (0.024–0.025). This could be explained by the differences in the titanias morphologies highlighted by comparing XRD and BET data (see Section 3.1): well-crystallized 5 nm anatase spheres for AK350 and larger nanospheres with intraparticle porosity for PC500 and UV100, where some gold particles can be located. In this configuration, these particles potentially lie buried below a titania layer thicker than the depth from which photoelectrons contributing to the XPS signal originate (few nm). Nevertheless, the Au/Ti surface atomic ratio is in all cases higher than the Au/Ti *bulk* atomic ratio calculated from ICP data (0.004–0.005), showing the high concentration of gold at the catalyst surface.

Chlorine is detected in the XPS spectra of all uncalcined materials (Table 4). The measured binding energy of the Cl $2p_{3/2}$ core level in all materials corresponds to that of the chloride anion (198.1 eV [30]). The Cl $2p_{3/2}$ peak can be attributed to the chloride interacting with the titania surface or to residual $AuCl_x$ species [31].

Sulfur is detected at the surface of all these high surface area catalysts, with a higher concentration (relative to gold) on the AK350 catalyst (Table 4). The Au/S surface atomic ratios are higher than the theoretical Au/S *bulk* atomic ratios (0.3–0.4), indicating that the sulfur concentration is lower at the surface of the catalyst than in the bulk. The S $2p_{3/2}$ peak is attributed to the presence of sulfate anions chemisorbed on the oxide support [32], probably as titanyl sulfates [33].

Sodium is detected in high concentration at the surface of Au/AK350 (Table 4). The Au/Na surface atomic ratio is lower than the

Au/Na bulk molar ratio (0.54). This is consistent with accumulation of sodium on the surface during gold deposition on the support, coming from the $NaBH_4$ reducing agent.

Boron is detected in high concentration at the surface of Au/UV100 (Table 4). As UV100 is initially free of boron, this shows that boron-containing species have reacted with the catalyst surface during the synthesis. Surface boron is in an oxidized state, as the binding energy of the B 1s core level is measured at 191.3 eV. This is higher than the binding energy of the 1s core level of B^0 (187.7 eV) and slightly lower than the binding energy of the B^{III} (in B_2O_3) 1s core level (193.5 eV) [34,35]. This is attributed to a strong interaction between B_2O_3 and the titania support [36].

3.2.5. Catalytic properties

The catalytic behaviors of these Au/TiO_2 materials are shown in Table 3. It is noted that, in the absence of a catalyst, the *trans*-stilbene oxide yield reached under these conditions is below 1% [10]. Actually, even in the presence of titania powders, both *trans*-stilbene conversions and epoxide yields are negligible, except in the case of UV100, on which the conversion reaches 15% (Table 2). However, this is below the activity of the Au/TiO_2 catalysts (26–64%, Table 3). Furthermore, only 2% epoxide is produced over pure UV100, vs. 20–44% on the gold catalysts, which gives a poor selectivity of 13% vs. 64–75% on the catalysts. This is a clear indication of the involvement of gold in the epoxide formation.

The activities of the titania-supported, 3 nm gold particles vary quite significantly in the following order: Au/UV100 > Au/PC500 > Au/AK350. Given that the dispersions of gold in these samples are similar, the turnover numbers vary in the same way. In 24 h, the turnover number of the reaction is higher on Au/PC500 than on Au/AK350 and higher on Au/UV100 than on Au/PC500. This can be explained by the morphologies of the titania supports and the chemical compositions of the catalyst surfaces, as will be discussed below. The TON reaches $680\,mol_{tS}^{-1}\,mol_{Ausurf}^{-1}$ on Au/UV100 in 24 h, which makes this catalyst slightly more active than the reference WGC catalyst ($620\,mol_{tS}^{-1}\,mol_{Ausurf}^{-1}$). On the other hand, selectivities are comparable for all catalysts, in the range 69–75%. These are slightly higher than that observed on the Au/P25 reference catalyst (Table 3) and higher than those reported for the epoxidation of styrene over Au/TiO_2 [37].

4. Discussion

4.1. On the effect of the titania morphology on the preparation of the catalysts

Although similar size distributions of gold are achieved on all the supports, the titania morphology seems to have an effect on the optical properties of gold as shown by UV–vis DRS. XPS experiments further show that (gold-modified) titania surfaces do not exhibit the same reactivity towards the species present in the preparation mixture ($HAuCl_4$, PVA, $NaBH_4$, ...).

4.2. On the effect of the titania morphology on the catalytic properties of the materials

It is interesting that the morphology of the anatase used (and the chemical surface composition of the resulting catalyst) more critically affects turnover numbers and epoxide yields than selectivity. The efficiencies of the titanias as supports for gold catalysts vary in the following order: AK350 < PC500 < UV100. Given that gold dispersions are similar on all supports and that the interaction between gold particles and the support are similar (XPS), the poor catalytic activity of Au/AK350 may arise from a poisoning effect by sodium, which is found in high concentration at the surface of this catalyst. The XPS study reveals indeed that the Au/AK350 surface bears four times more sodium atoms than gold atoms (Table 4). It is also possible that, although the bare supports exhibit only limited activity for stilbene epoxidation (Table 2), the surface titanol groups take part in the epoxidation mechanism and that they promote the gold-catalyzed stilbene transformation. The hydroxyl-deficient AK350 surface (Fig. 1, Table 2) would thus be less efficient than PC500 and UV100. The superiority of Au/UV100 over Au/PC500 could be explained by the presence of boron oxide on the catalyst surface (Table 4), which could enhance the epoxidation reaction. Boron trichloride has indeed been reported to promote the gas phase oxidation of hydrocarbons with molecular oxygen [38] while alumina-boria catalysts can partially oxidize ethane to acetaldehyde using air as the oxidant [39]. It is thus possible that boron oxide promotes reactions involving oxygen-centered free-radicals [40]. Further work is in progress in order to determine the extent of promotion of the gold-catalyzed epoxidation of stilbene by titanols and boron oxide and to identify the steps in the proposed reaction mechanism [10] which they actually accelerate. It is interesting that chemical promotion effects can compensate for the accepted very favorable gold–P25 interaction in the WGC catalyst [41], thereby making Au/UV100 more active than the reference catalyst.

5. Conclusions

We have shown that the colloidal deposition method yields similar gold dispersions (>40%) over anatase titanias with similar surface areas, despite the very different morphologies of the bare supports. The well-crystallized, less hydroxylated AK350 support leads to the least active gold catalyst, while Au/UV100 turns out to be the best catalyst. Given that gold particles experience similar interaction with all supports, as shown by XPS studies, the superiority of Au/PC500 and Au/UV100 are related to chemical promotion of the gold-catalyzed stilbene epoxidation by titanol groups, with an additional promotion by boron oxide in the case of Au/UV100. On the other hand, selectivities are basically unaffected by the titania morphology and surface composition of the resulting catalyst. Finally, it seems that the chemical promotion of the reaction can compensate for the otherwise determining metal–support interaction in Au/P25. This makes Au/UV100 more efficient for the epoxidation of stilbene than the Au/TiO_2-P25 reference catalyst from WGC.

Acknowledgements

The authors wish to acknowledge funding from the IDECAT Network of Excellence of the 6th European Framework Program and thank B. Jouguet for TG–DTA analyses, L. Massin for XPS measurements, Dr G. Bergeret and M.-T. Gimenez for XRD, P. Mascunan and N. Cristin for ICP, P. Chaney for TEM pictures.

References

[1] M.G. Clerici, G. Bellussi, U. Romano, J. Catal. 129 (1991) 159.
[2] M.G. Clerici, P. Ingallina, J. Catal. 140 (1993) 71.
[3] R.A. Sheldon, J. Dakka, Catal. Today 19 (1994) 215.
[4] O.A. Kholdeeva, A.Yu. Derevyankin, A.N. Shmakov, N.N. Trukhan, E.A. Paukshtis, A. Tuel, V.N. Romannikov, J. Mol. Catal. A 158 (2000) 417.
[5] A. Tuel, L.G. Hubert-Pfalzgraf, J. Catal. 217 (2003) 343.
[6] E. Jorda, A. Tuel, R. Teissier, J. Kervennal, J. Chem. Soc. Chem. Commun. (1995) 1175.
[7] E. Jorda, A. Tuel, R. Teissier, J. Kervennal, J. Catal. 175 (1998) 93.
[8] P. Lignier, F. Morfin, S. Mangematin, L. Massin, J.-L. Rousset, V. Caps, Chem. Commun. (2007) 186.
[9] Gold reference catalysts, Gold Bull. 36 (2003) 24.
[10] P. Lignier, F. Morfin, L. Piccolo, J.-L. Rousset, V. Caps, Catal. Today 122 (2007) 284.
[11] M. Comotti, W.-C. Li, B. Spliethoff, F. Schüth, J. Am. Chem. Soc. 128 (2006) 917.

[12] H. Tahiri, N. Serpone, R. Le van Mao, J. Photochem. Photobiol. A 93 (1996) 199.
[13] P. Pichat, H. Courbon, R. Enriquez, T.T.Y. Tan, R. Amal, Res. Chem. Intermed. 33 (2007) 239.
[14] K.Y. Ho, K.L. Yeung, Gold Bull. 40 (2007) 15.
[15] J. Kirchnerova, M.-L. Herrera Cohen, C. Guy, D. Klvana, Appl. Catal. A 282 (2005) 321.
[16] V. Caps, Y. Wang, J. Gajecki, B. Jouguet, F. Morfin, A. Tuel, J.-L. Rousset, Stud. Surf. Sci. Catal. 162 (2006) 127.
[17] R. Van Hardeveld, F. Hartog, Surf. Sci. 15 (1969) 189.
[18] D.G. Duff, A. Baiker, in: G. Poncelet, J. Martens, B. Delmon, P.A. Jacobs, P. Grange (Eds.), Preparation of Catalysts VI, Elsevier, Amsterdam, 1995 , p. 505 (Stud. Surf. Sci. Catal. 91 (1995) 505).
[19] D. Buso, J. Pacifico, A. Martucci, P. Mulvaney, Adv. Funct. Mater. 17 (2007) 347.
[20] Y.F. Han, Z. Zhong, K. Ramesh, F. Chen, L. Chen, J. Phys. Chem. C 111 (2007) 3163.
[21] M. Haruta, N. Yamada, T. Kobayashi, S. Iijima, J. Catal. 115 (1989) 301.
[22] A.M. Visco, F. Neri, G. Neri, A. Donato, C. Milone, S. Galvagno, Phys. Chem. Chem. Phys. 1 (1999) 2869.
[23] P. Heimann, J.F. Van der Veen, D.E. Eastman, Solid State Commun. 38 (1981) 595.
[24] S. Arrii, F. Morfin, A.J. Renouprez, J.-L. Rousset, J. Am. Chem. Soc. 126 (2004) 1199.
[25] H.-P. Steinrück, F. Pesty, L. Zhang, T.E. Madey, Phys. Rev. B 51 (1995) 2427.
[26] L. Óvári, J. Kiss, Appl. Surf. Sci. 252 (2006) 8624.
[27] A.F. Carley, P.R. Chalker, J.C. Rivieret, M.W. Roberts, J. Chem. Soc., Faraday Trans. 1 83 (1987) 351.
[28] T. Matsumoto, M. Batzill, S. Hsieh, B.E. Koel, Surf. Sci. 572 (2004) 127.
[29] Y. Xie, Q. Zhao, X.J. Zhao, Y. Li, Catal. Lett. 118 (2007) 231.
[30] H. Yun, J. Li, H.-B. Chen, C.-J. Lin, Electrochim. Acta 52 (2007) 6679.
[31] A. Kumar, S. Mandal, P.R. Selvakannan, R. Pasricha, A.B. Mandale, M. Sastry, Langmuir 19 (2003) 6277.
[32] T.W. Schlereth, M.N. Hedhili, B.V. Yakshinskiy, T. Gouder, T.E. Madey, J. Phys. Chem. B 109 (2005) 20895.
[33] C. Xie, Q. Yang, Z. Xu, X. Liu, Y. Du, J. Phys. Chem. B 110 (2006) 8587.
[34] M.M. Ennaceur, B. Terreault, J. Nucl. Mater. 280 (2000) 33.
[35] M.X. Wang, A. Yoshikawa, H. Miyauchi, T. Nakahata, Y. Oya, N. Noda, K. Okuno, J. Nucl. Mater. 367–370 (2007) 1503.
[36] T. Yuzhakova, V. Rakić, C. Guimon, A. Auroux, Chem. Mater. 19 (2007) 2970.
[37] N.S. Patil, B.S. Uphade, P. Jana, R.S. Sonawane, S.K. Bhargava, V.R. Choudhary, Catal. Lett. 94 (2004) 89.
[38] G.A. Kapralova, V.G. Fedotov, A.M. Chaikin, Doklady Chem. 397 (2004) 165.
[39] G. Colorio, J.C. Védrine, A. Auroux, B. Bonnetot, Appl. Catal. A 137 (1996) 55.
[40] P. Renaud, A. Beauseigneur, A. Brecht-Forster, B. Becattini, V. Darmency, S. Kandhasamy, F. Montermini, C. Ollivier, P. Panchaud, D. Pozzi, E. Martin Scanlan, A.-P. Schaffner, V. Weber, Pure Appl. Chem. 79 (2007) 223.
[41] M. Haruta, CATTECH 6 (2002) 102.